10º Congreso de Exploración y Desarrollo de Hidrocarburos
Simposio de Evaluación de Formaciones: Maximizando la eficiencia a través de la innovación

A PROPOSED WORKFLOW FOR ESTIMATING ANISOTROPIC ELASTIC PROPERTIES FOR VACA MUERTA FORMATION

Pablo Pateti[1], Dr. Alexis Ortega[2]

1: Wintershall Energía S.A., pablo.pateti@wintershall.com

2: Wintershall Holding GmbH, alexis.ortega@wintershall.com

Keywords: **elastic moduli, Vaca Muerta Formation**

RESUMEN

Un flujo de trabajo propuesto para la estimación de propiedades elásticas anisotrópicas para la Formación Vaca Muerta.

Comúnmente, las lutitas se caracterizan como rocas transversalmente isotrópicas, para lo que se requiere el conocimiento de cinco coeficientes de rigidez independientes. Los perfiles de pozo (densidad y sónico) no proveen la suficiente información para estimar todos los coeficientes del tensor de rigidez. Es posible obtener estos coeficientes a partir de ensayos de laboratorio en muestras de coronas (tapones) orientados en diferentes direcciones respecto de las laminaciones. Sin embargo, es necesario propagar a lo largo de la trayectoria del pozo estos valores discretos medidos en laboratorio, de manera de poder aplicar estos resultados en cualquier flujo de trabajo para caracterización de reservorios. En el caso de la Formación Vaca Muerta, el método usado comúnmente consiste en complementar las constantes elásticas estimadas a partir de perfiles de pozo con correlaciones empíricas basadas en datos de laboratorio para estimar el tensor de rigidez completo. Sin embargo, este método solo puede aplicarse en caso de pozos verticales u horizontales, y requiere el uso de perfiles de pozo originales.

En el presente trabajo se propone un flujo de trabajo para la estimación del tensor de coeficientes elásticos de rigidez para el caso de una roca transversalmente isotrópica, integrando resultados de la evaluación petrofísica con conceptos de física de rocas. Esto ayuda a incorporar tanto información sobre la composición de la roca como características texturales. El flujo de trabajo puede ser aplicado para pozos de cualquier trayectoria, siempre que haya disponibles resultados de una evaluación petrofísica. Los resultados principales son propiedades elásticas anisotrópicas: Modulo de Young y relación de Poisson. Adicionalmente, se puede estimar el coeficiente de Biot para el caso anisotrópico. El flujo de trabajo permite reconstruir tanto el perfil de densidad como los perfiles sónicos (compresional y de corte) en las direcciones perpendicular y paralela a las laminaciones. Los resultados obtenidos a partir de esta metodología fueron aplicados en la simulación de fracturamiento hidráulico. El buen ajuste obtenido en el historial de presiones de tratamiento, geometría de fractura y producción post fractura nos brindan confianza sobre la robustez del método propuesto.

INTRODUCTION

A detailed assessment of petrophysical and geomechanical properties is required for appraising and developing organic-richshale formations. Assessment of elastic properties in this type of formations can be quite challenging due to complex mineralogy and anisotropy. Empirical models based on correlations from core data have been developed and well log measurements have been used to assess the complete stiffness tensor for a vertically-transverse isotropic (VTI) medium (Figure 1).

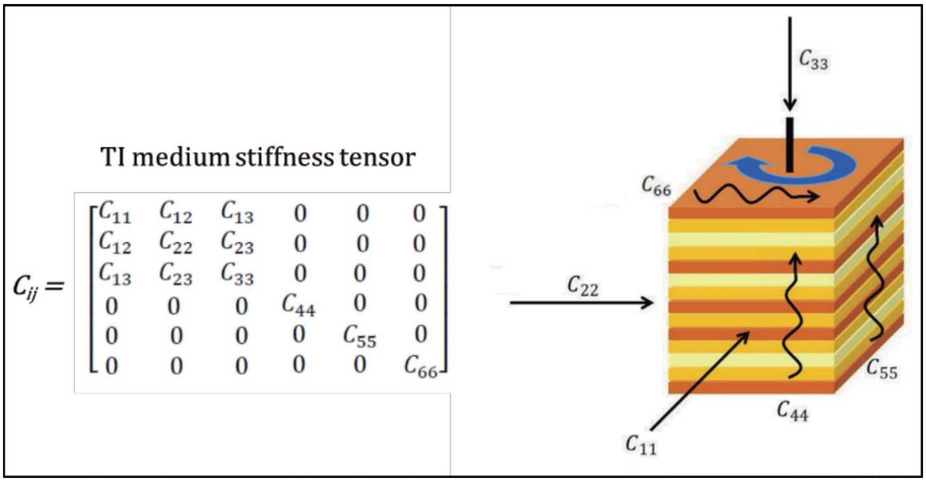

Figure 1. Stiffness coefficient tensor for a vertically-transverse isotropic medium (modified from Willis 2013).

Traditional methods use density and acoustic travel time measurements from well logs complemented by core-based correlations to estimate the tensor components (Quirein *et al.* 2014; Massaro *et al.* 2017). For a vertical well (Figure 2), assuming VTI behavior, the bedding-normal stiffness coefficients C_{33} and C_{44} (equal to C_{55}) are calculated from the compressional and fast/slow shear velocities, respectively. C_{11} (equal to C_{22}) and C_{66} correspond to the compressional and shear modulus in the horizontal plane. There is no logging tool that allows their measurement. However, C_{66} can be obtained from processing of the Stoneley wave (Tang and Patterson 2004).

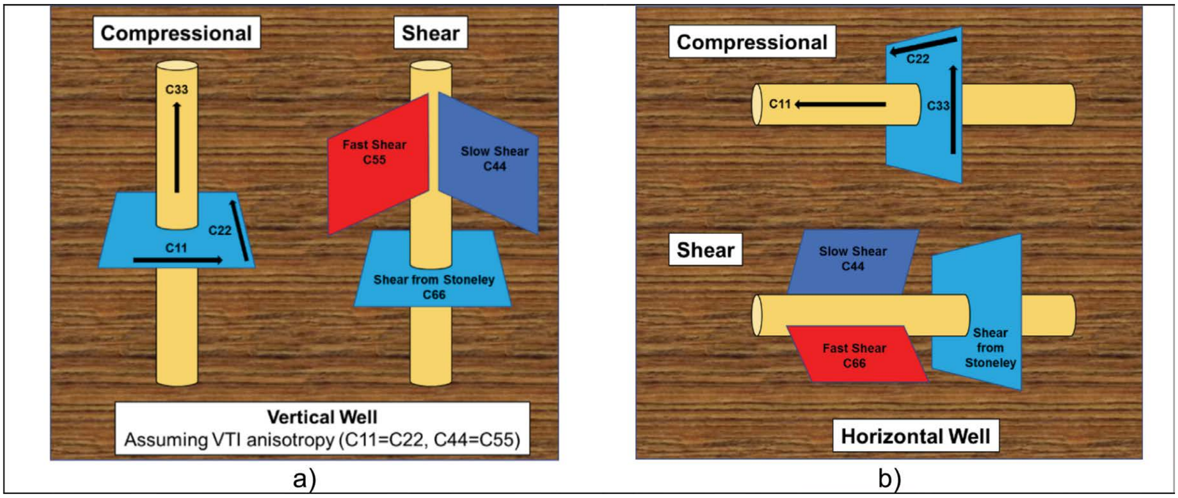

Figure 2. Stiffness coefficients depending on well deviation(Modified from Schlumberger, 2015).

For this, the Stoneley data must be compensated for tool effects, C_{66} must be estimated outside any near-wellbore altered annulus, and mud density and velocity must be accurately determined (Tang and Patterson 2004; Walsh *et al.* 2006).

In the case of a horizontal well, C_{11} is calculated directly from the compressional velocity as in the case of the vertical well (Figure 2). The fast and slow shear are used to compute C_{66} and C_{44}, respectively. Dipole data (e.g. xx and yy dipoles) can be used to compute C_{44} and C_{66}, provided that the tool does not rotate and that is perfectly aligned with the horizontal and vertical earth axis. Otherwise, fast and slow shear would need to be derived from Alford rotation to obtain the true fast and slow shear.

Prioul *et al.* (2016) presented a method based on measurements on cuttings and petrophysical and rock physics models for predicting anisotropic mechanical properties and stresses in the Vaca Muerta Formation, especially for the case of horizontal wells where well logs are not available. In their workflow, they present a rock physics model, which uses the results from an empirical petrophysical volumetric model as input to predict C_{33}, C_{55} (equal to C_{44} in VTI case) and C_{66}. The other stiffness coefficients (C_{11}, C_{12}, C_{13}) are estimated using empirical correlations based on results from core analysis.

Similar to Prioul *et al.*, we propose an alternative workflow that does not rely on original logs for estimating elastic stiffness coefficients for a VTI case. Instead, these are estimated using the results from the petrophysical analysis (matrix components, porosity, fluids) in combination with rock physics-based methods, which allows for incorporating both compositional and textural characteristics. On the other hand, unlike Prioul *et al.*, the workflow proposed heredoes not rely on empirical correlations for deriving C_{11}, C_{12} and C_{13}, to estimate the complete elastic stiffness coefficient tensor, as these coefficients are obtained using rock physics-based methods, as mentioned above. In addition, the current studyuses different methods for incorporating porosity and fluids into the elastic moduli estimation. The proposed formulation will be explained in more detail in the next sections of the document.

The workflow presented in this study allows for estimating the values for Young's Modulus, Poisson's ratio and Biot's coefficient for both parallel and perpendicular to bedding directions. The workflow also allows for reconstructing both density and compressional and shear travel times (normal and parallel to bedding). This workflow offers the following advantages:

- Additional QC for original well logs (bulk density and compressional and shear travel times).
    - Curve reconstruction in those intervals where original data is missing and/or affected by poor borehole conditions (e.g. washouts, rugosity), inaccuracies in log processing (i.e. inaccurate picking of arrival times in intervals with poor semblance), and changes in mud properties with depth (i.e. for Stoneley wave processing).

- Increased consistency between elastic properties and petrophysical evaluation.
  - Modelled data will have the same resolution as the results from the petrophysical analysis. This reduces additional errors due to depth mismatch between log measurements and/or differences in vertical resolution.
- Consideration of fluid effects
  - Allow for calculating the response of logs to different fluid saturation conditions. This is particularly useful for correcting log responses for hydrocarbon effects (i.e. gas) and mud filtrate invasion.

PETROPHYSICAL INTERPRETATION

The wells used for this study have an extensive suite of logs and core measurements. A summary of the data used specifically for this work is presented in Table 1. The results from the petrophysical interpretation were cross checked with measurements from advanced logging tools (Nuclear Magnetic Resonance, Dielectric dispersion) and results from laboratory analysis on cores and cuttings samples.

Well Logs	Core Analysis
-Gamma Ray (total and Spectral) -Induction Resistivity -Bulk Density and Photoelectric factor -Neutron Porosity -Cross-Dipole Sonic (Pre- and Post-Frac) -Micro-Resistivity Image -Neutron-Induced Elemental Capture Spectroscopy -Nuclear Magnetic Resonance (NMR) -Dielectric Dispersion	-Gamma Ray (total and Spectral) -Mineralogy (X-Ray Diffraction, X-Ray Fluorescence, Fourier Transform Infrared Spectroscopy) -Geochemistry (Pyrolysis, Rock Eval) -Retort Analysis (Total and Effective porosities and fluid saturations, grain Density, Clay-bound Water, Pulse and Pressure Decay Permeability). -Rock Mechanics (Multi stress path compression tests, ultrasonic velocity measurements)

Table 1. Well Log and core data used specifically for this study.

The petrophysical analysis is based on aprobabilistic multi-mineral model, from which matrix volumes, porosity and fluids saturations are obtained. Well logs are used as inputs, and the model's outputis compared with core data. The results from the petrophysical analysis are shown in Figure 3.

Mineralogy

The mineral model consists of quartz-feldspars-mica (QFM), calcite, dolomite, clays (illite being the dominant type), pyrite and kerogen. Mineralogy and TOC (Total Organic Carbon) were obtained from elemental spectroscopy logs and used as input for the multi-mineral model. These show a good

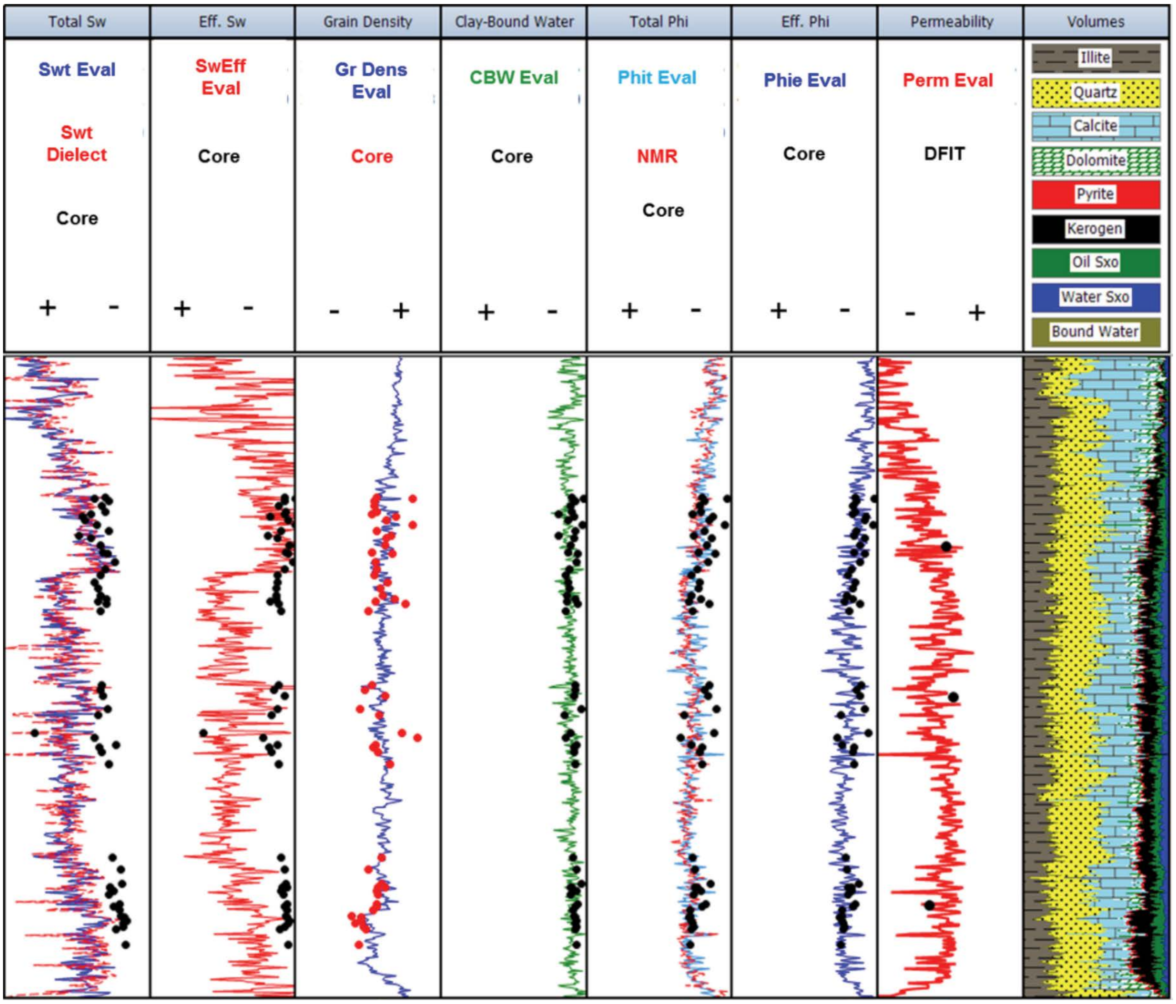

Figure 3. Results from petrophysical analysis.

agreement with results from cores and cuttings, as shown in Figure 4a. The vertical variation of mineralogy and TOC throughout the Vaca Muerta section is evident. Throughout the Vaca Muerta Formation, the mineral components show distinctive trends with depth, especially QFM, carbonates and TOC. On both a depth plot (Figure 4a) and a ternary plot (Figure 4b), it is evident that total carbonate and QFM contents are inversely proportional (one increase while the other decreases), and show a greater variation when compared to clay content.This is in line with observations from previous studies (Marchal *et al.* 2016; Cuervo *et al.* 2016). The carbonate content (being calcite the dominant component) ranges between 20wt% to 45wt% (P10 and P90 values, respectively) and increases towards the top of the Vaca Muerta section. QFM ranges between 20wt% to 34wt% (P10 and P90 values, respectively) and increases towards the base of the Vaca Muerta section where the carbonate content tends to decrease. Clay content is generally lower than 35wt%, and remains fairly constant averaging around 25wt%. TOC increases from 2wt% to 7wt% (on average) towards the bottom of the section. Pyrite increases with TOC, and generally is below 5wt%.

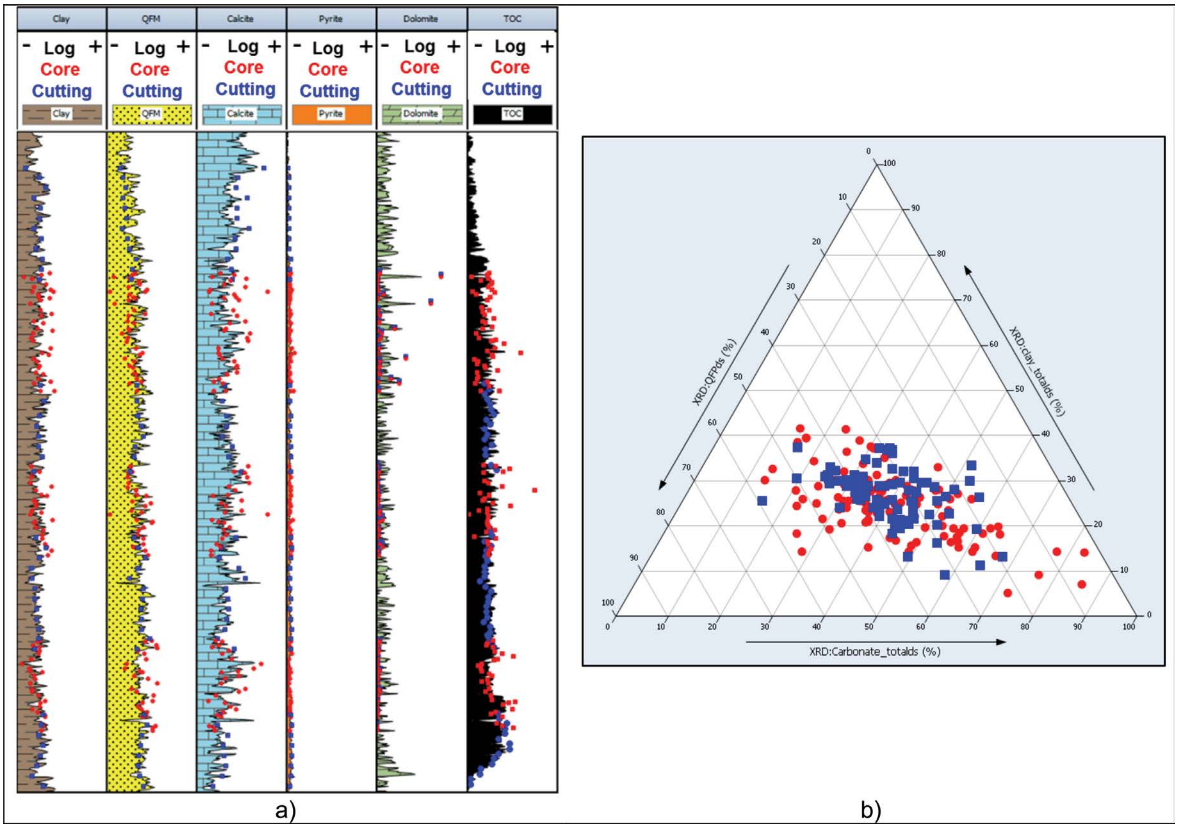

Figure 4. a) Comparison between elemental capture spectroscopy logs and XRD and TOC; b) Ternary plot.

Porosity

Total porosity is calculated from combining the responses of Density and Neutron logs, and correcting for the presence of organic matter. Results showed a good match with both total porosity from Nuclear Magnetic Resonance (NMR) and results from continuous (multi-stage) retort measurements on crushed samples. Clay-bound water was also used as another input for the petrophysical analysis, used to make an additional correction to total porosity in order to obtain a clay-corrected porosity. Clay-bound water measured on cores through a continuous retort process is consistent with clay content from X-ray diffraction. A correlation was established (Figure 5).

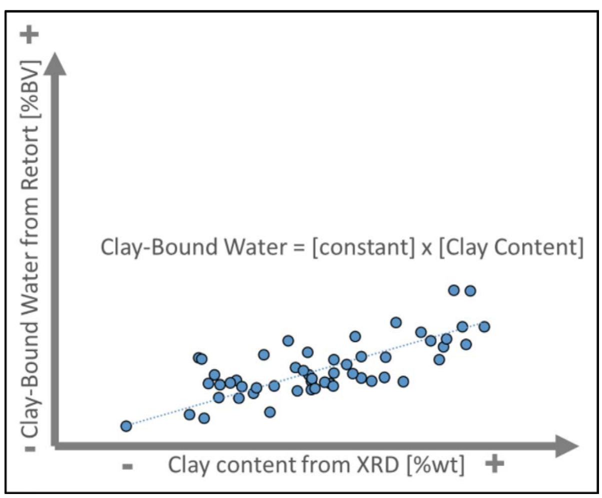

Figure 5. Correlation between clay-bound water from retort measurements and total clay content from XRD.

Water Saturation

Water saturation was calculated using Archie's formula for total porosity (Eq. 1):

$$SwT = \sqrt[n]{\frac{a * Rw}{Rt * \varnothing_T^m}} \qquad (1)$$

Values for m and n were obtained from inversion of NMR and dielectric dispersion measurements. The water volume derived from dielectric dispersion measurements was used as the reference for comparison. As shown in Figure 3, the results agree with the bulk volume water from dielectric dispersion measurements. Clay-bound water was used for correcting the total water saturation for clay content. Results show a good agreement with results from core for 2/3 of the upper cored section. For the rest of the core sections, results from core are consistently lower than those obtained from the petrophysical analysis. This was likely due to incorrect handling procedures in the laboratory.

Permeability

Permeability was calculated from the NMR log using the Logarithmic mean of the T2 distribution. The results were calibrated with system permeability interpreted from G-function analysis of Diagnostic Fracture Injection Tests (DFIT).

PROPOSED WORKFLOW

The proposed workflow is shown in Figure 6. The results from the petrophysical analysis are used as inputs: minerals and kerogen volumes, total porosities and water saturation. The main outputs are the anisotropic Young's Modulus, Poisson's ratio and Biot's coefficient. Bulk Density, compressional and shear travel times (in the directions normal and perpendicular to bedding) are reconstructed by combining the results from the petrophysical analysis and the estimated elastic properties. This curve reconstruction serves as a mean for calibrating the results as well as an additional tool to assess the quality of the original well logs.

A key element in the proposed workflow is the modelling of the influence of kerogen on the anisotropy of organic-rich shales. Previous studies (Vernik and Nur 1992; Vernik *et al.* 1994; Vernik and Landis 1996; Vernik and Liu 1997) have shown that these rocks exhibit a high level of anisotropy, which is primarily related to the lenticular distribution of kerogen and clay-mineral-preferred orientation parallel to the bedding plane. Anisotropy is further enhanced by bedding-parallel microcracks, which can survive *in-situ* stress specially in highly overpressured shales (Vernik and Milovac 2011). The same studies demonstrated that anisotropy increases with

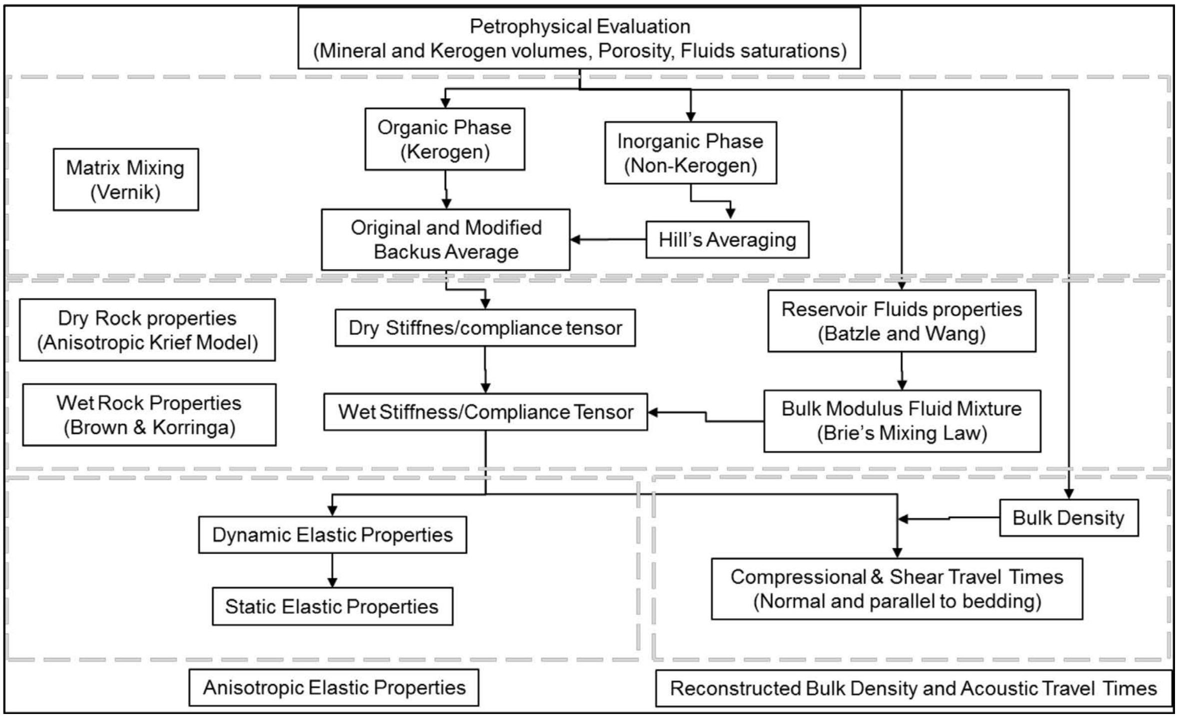

Figure 6. Proposed Worflow.

the bulk kerogen content, since organic materials tend to be more compliant than other matrix components.

The data shown in Figure 7 is part of the rock mechanics core analysis data set that is available for the Vaca Muerta Formation in the study area. It is shown that the increase in bulk kerogen volume not only causes a reduction on the elastic stiffness but also increases the anisotropy. These results are consistent with findings from previous studies.

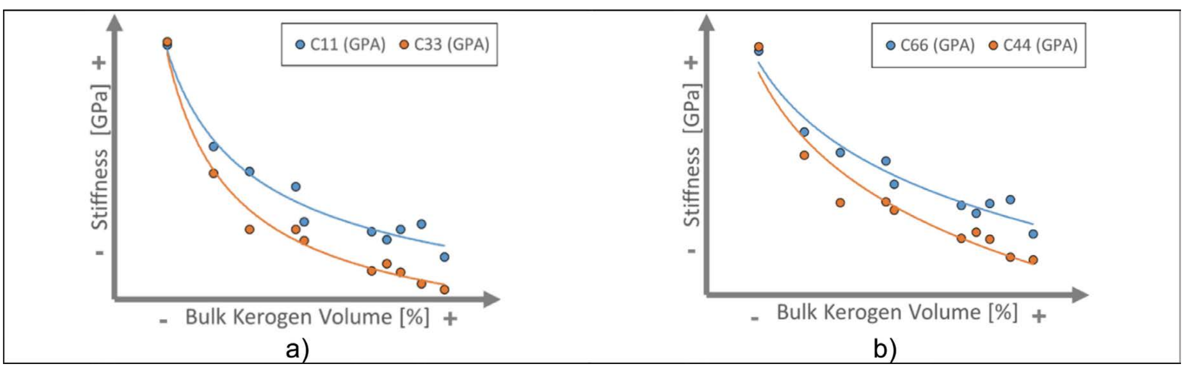

Figure 7. Influence of kerogen content in and elastic stiffness coefficients.

The first step in the workflow is defining the matrix properties. The solid matrix is modelled as a mixture of organic (kerogen) and inorganic (non-kerogen) phases. The stiffness of the inorganic phase is computed using Hill's average for mixing the different components (Yenugu and Vernik 2015). For mixing the organic and inorganic phases, we consider the Backus average model (Backus 1962), which describes a rock composed of a periodic repetition of a two-layer composite of kerogen and non-kerogen (Vernik and Nur 1991; Carcione and Avseth 2015). This model yields the elastic constants that describe the properties of a layered transversely-isotropic medium (Eq. 2 to 7):

$$C_{11} = \langle c_{11}\rangle + \langle c_{33}^{-1}\, c_{13}\rangle^2 \langle c_{33}^{-1}\rangle^{-1} - \langle c_{33}^{-1}\, c_{13}^2\rangle \quad (2)$$

$$C_{33} = \langle c_{33}^{-1}\rangle^{-1} \quad (3)$$

$$C_{12} = C_{11} - \langle c_{11}\rangle + \langle c_{12}\rangle \quad (4)$$

$$C_{13} = \langle c_{33}^{-1}\, c_{13}\rangle \langle c_{33}^{-1}\rangle^{-1} \quad (5)$$

$$C_{44} = \langle c_{44}^{-1}\rangle^{-1} \quad (6)$$

$$C_{66} = \langle c_{66}\rangle \quad (7)$$

Where, C_{ij} correspond to the elastic stiffness coefficients of the transverse isotropic medium and cij represent the constants for the individual components (kerogen and non-kerogen). The brackets refer to volume-weighted averages of the two components.

It has been observed that as kerogen content increases, the Backus model increasingly over predicts the bedding-parallel stiffness coefficients (Vernik and Landis 1996; Vernik and Nur 1992; Vernik 2016; Sayers 2013), as shown in Figure 8. Vernik and Liu (1997) introduced a heuristic modification of the Backus model that only affects the bedding-parallel stiffness coefficients (C_{11} and C_{66}). This modification is based on scanning electron microscopy (SEM) observations, which show that the clay fabric exhibits a lenticular pattern rather than a continuous layer structure (Vernik and Nur 1992; Sayers 2013; Carcione and Avseth 2015). The modification only affects the bedding-parallel elastic constants, by replacing them with the weighted average that takes into account the local proportions of kerogen and non-kerogen (Carcione and Avseth 2015), as follows (Eq. 8 to 13):

$$C_{11} = \alpha M + (1-\alpha) N \quad (8)$$

$$C_{66} = \alpha P + (1-\alpha) Q \quad (9)$$

$$M = \langle c_{11}\rangle + \langle c_{33}^{-1}\, c_{13}\rangle^2 \langle c_{33}^{-1}\rangle^{-1} - \langle c_{33}^{-1}\, c_{13}^2\rangle \quad (10)$$

$$N = \langle c_{11}^{-1}\rangle^{-1} \quad (11)$$

$$P = \langle c_{66}\rangle \quad (12)$$

$$Q = \langle c_{66}^{-1} \rangle^{-1} \tag{13}$$

Where, α is an empirical constant that accounts for the degree of lateral discontinuity of the shale laminae (Vernik and Liu 1997); M and P corresponds to C_{11} and C_{66} as calculated from the original Backus average equation, and N and Q have the same structure as C_{33} and C_{44} from the Backus average.

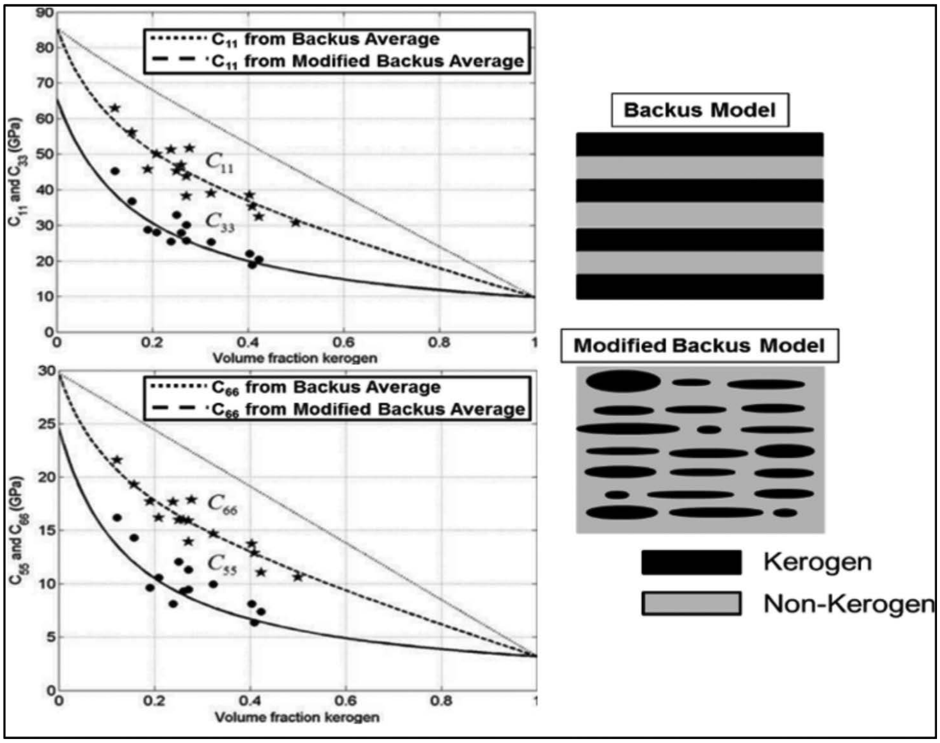

Figure 8. Elastic stiffness coefficients computed from bedding-parallel and bedding-normal ultrasonic velocities measurements reported by Vernik and Liu (1997) compared with the original and modified Backus average models (modified from Sayers 2013).

For the dry frame properties, we adopted the anisotropic version of the Krief *et al.* (1990) model presented by Carcione and Avseth (2015), as shown in Eq. 14 to 18:

$$c_{11}^{dry} = c_{11}^{m}\, g(A) \tag{14}$$

$$c_{66}^{dry} = c_{66}^{m}\, g(A) \tag{15}$$

$$c_{13}^{dry} = c_{13}^{m}\, g(B) \tag{16}$$

$$c_{33}^{dry} = c_{33}^{m}\, g(B) \tag{17}$$

$$c_{44}^{dry} = c_{44}^{m}\, g(B) \tag{18}$$

Where g(x) is given by Eq. 19 below, and A and B are constants (A<B).

$$g(x) = (1-\emptyset)^{x/(1-\emptyset)} \qquad (19)$$

The use of two constants is somehow equivalent to vary the Krief exponent as a function of the propagation (phase) angle, since c_{11}^{m} and c_{66}^{m} describe the velocities along the stratification, and c_{33}^{m} and c_{44}^{m} along the perpendicular direction (Carcione and Avseth 2015). These constants are calibrated using both cores and well logs from both vertical and horizontal wells.

Dry stiffness coefficients are turned into compliances tensor elements using the equations presented by Mavko *et al.* (2003). The elastic constants of a saturated medium can be predicted using the method proposed by Brown and Korringa (1975), given by Eq. 20:

$$S_{ijkl}^{sat} = S_{ijkl}^{dry} - \frac{\left(S_{ijaa}^{dry} - S_{ijaa}^{min}\right)\left(S_{bbkl}^{dry} - S_{bbkl}^{min}\right)}{\left[\left(S_{ccdd}^{dry} - S_{ccdd}^{min}\right) + \emptyset_T\left(\frac{1}{K_{fl}} - \frac{1}{K_{min}}\right)\right]} \qquad (20)$$

Where S_{ijkl}^{min}, S_{ijkl}^{dry} and S_{ijkl}^{sat} are the elastic compliance tensor of the mineral matrix, dry and saturated rock, respectively; $\emptyset_T$ is the total porosity; K_{fl} and K_{min} represent the bulk moduli of the pore fluid and mineral matrix, respectively. The properties of the individual fluids (i.e. density and bulk moduli) were calculated using the results from PVT analysis and the equations proposed by Batzle and Wang (1992), and the bulk moduli of the fluid mixture (K_{fl}) is calculated using a mixing law proposed by Brie *et al.* (1995).The elastic compliance tensor of the saturated rock is used for calculating the elastic stiffness coefficient tensor and the anisotropic Young's modulus and Poisson's ratio. The results are calculated considering in-situ fluid saturations (as obtained from the petrophysical analysis) and assuming fully water-saturated conditions (in an attempt to correct for hydrocarbon presence). The anisotropic Biot's coefficient is calculated based on dry and mineral matrix stiffness coefficients (Mavko *et al.* 2003).

Dynamic Young's Modulus was converted to a static value using a correlation presented by Canady (2011). Static Poisson's ratio was assumed to be equal to the dynamic value.

Bulk Density is reconstructed based on the results from the petrophysical analysis. It is calculated analytically, as a volumetric-weighted average of matrix and fluid densities as follows:

$$\rho_b = \rho_m(1-\emptyset_T) + \rho_{fl}\,\emptyset_T \qquad (21)$$

Where, ρ_b, ρ_m, ρ_{fl} are the bulk, mineral (dry) and fluid densities, respectively, and $\emptyset_T$ is total porosity. The reconstructed bulk density, together with the estimated elastic stiffness coefficients were used to reconstruct the compressional and shear travel times for both normal and parallel to bedding directions.

RESULTS

The results for dynamic elastic stiffness coefficients obtained using the workflow are shown in Figure 9 (tracks 2 through 7). Results are consistent with the vertical variation in porosity and mineralogy. Overall, higher stiffness values towards the top of the section, while lower values are found towards the bottom. Elastic stiffness increase with increasing carbonate content and, subsequently, reduction in porosity. Lower values of stiffness are related to increase in organic matter content and increase porosity. When compared with core measurements (red dots), modelled elastic stiffness coefficients are generally lower. This difference is thought to be due to the different measurement frequencies and sample volume between laboratory and well logs. Despite this difference, modelled curves show similar trends as the core measurements.

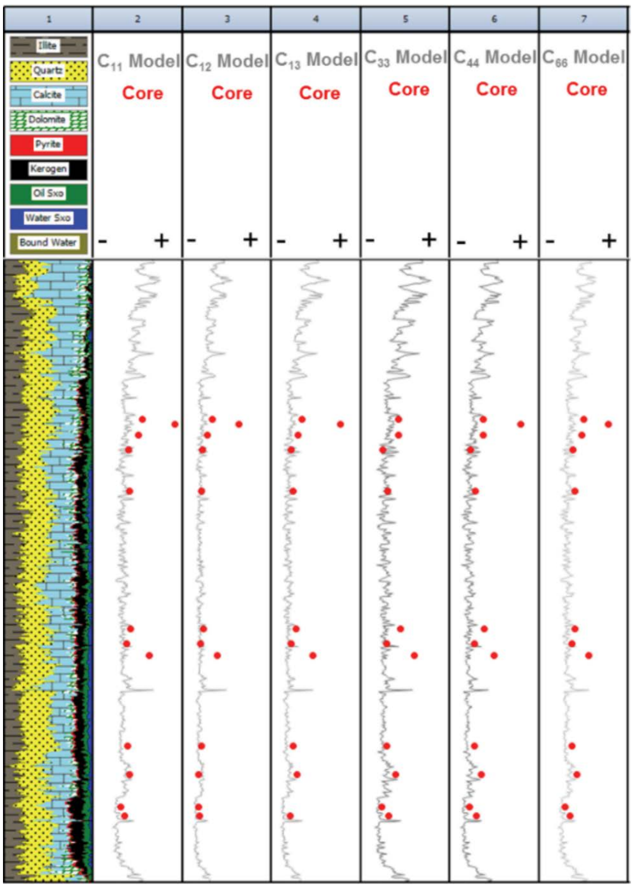

Figure 9. Modelled dynamic elastic stiffness coefficients compared with core measurements.

Figure 10 shows the reconstructed bulk density,along with the compressional and shear travel time curves (normal and parallel to bedding). As shown in tracks 2 through 6, modelled curves (red curves) show a good agreement with the original well logs (black curves). Bulk density (track

2) corresponds with the core measurements (points). In track 6, the modelled horizontal (parallel to bedding) shear travel time (red curve) shows a good agreement with the one estimated from Stoneley wave processing (black curve). Also, the modelled horizontal shear travel time has a higher resolution than the one from Stoneley wave processing.In general, both modelled and original travel times show higher values than those measured from core, similarly as with elastic stiffness coefficients. The difference is thought to be due to the different measurement frequencies and sample volume between laboratory and well logs. Despite this difference, both original and modelled curves show similar trends as the core measurements. Track 7 shows the Thomsen's Epsilon and Gamma parameters that describe the anisotropy of compressional and shear travel time, which tends to increase toward the base of the Vaca Muerta section where kerogen content increases, and tends to decrease towards the top where the carbonate content increases (with the subsequent reduction in porosity). Tracks 8 through 12 show the results for dynamic Young's Modulus, Poisson's ratio and Biot's coefficient. The last two tracks show the results for Static Young's modulus and Poisson's ratio. A reasonable match is observed between the model elastic properties and the results from core analysis.

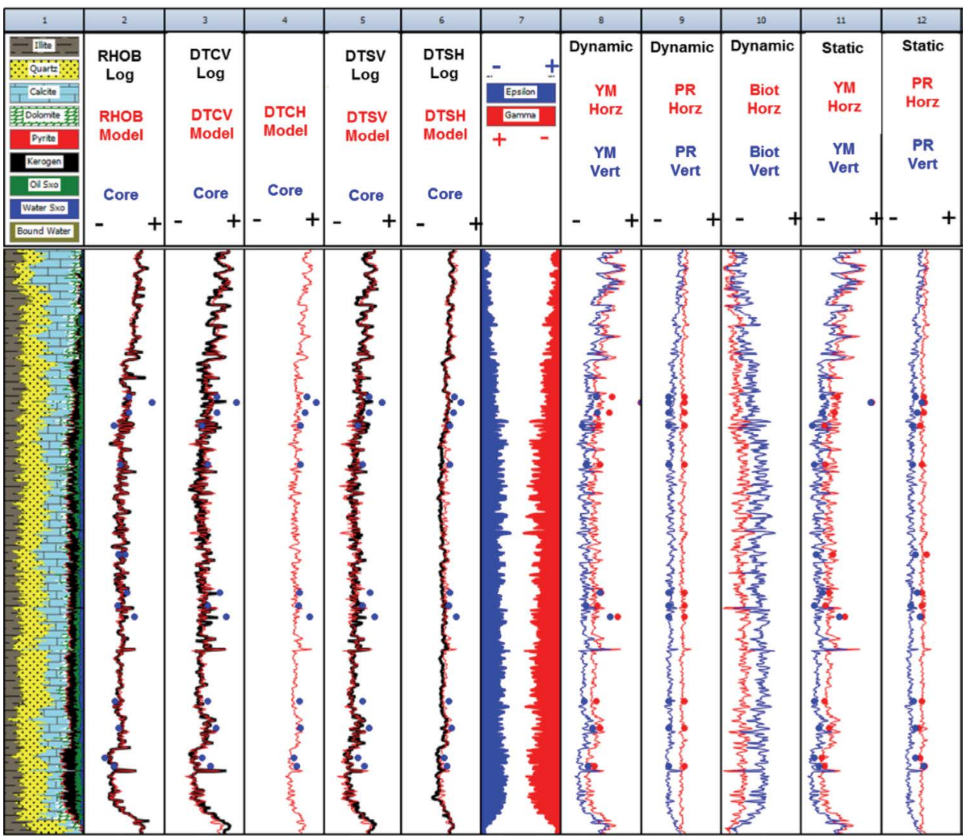

Figure 10. Tracks 2 through 6: Reconstructed bulk density, Compressional and Shear travel times (normal and parallel to bedding) compared with core measurements and original well logs; Track 7: Thomsen's Epsilon and Gamma parameters; Tracks 8 through 12: Dynamic and Static Anisotropic Young's Modulus and Poisson's ratio compared with core measurements, and dynamic Biot's coefficient.

APPLICATION TO HYDRAULIC FRACTURING

Results from petrophysical analysis (Fig. 3) along with the estimated static rock elastic properties (Fig. 10), including Young's Modulus, Poisson's Ratio and Biot's constant, were used as input data for the hydraulic fracturing simulation (Fig. 11). In this study, a planar three-dimensional geometry fracture simulator was used to build the hydraulic fracture models. Model calibration and validation of the results were carried out through pre-fracture tests analysis, treating pressure match, fracture geometry estimation, and production analysis.

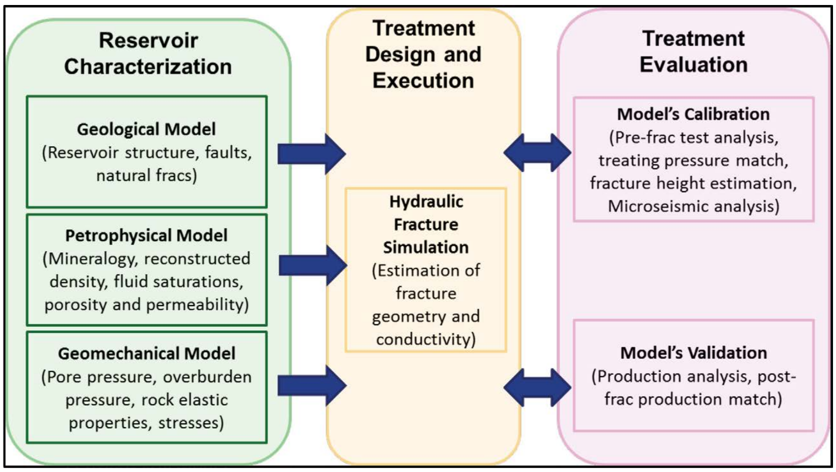

Figure 11. Hydraulic fracturing modeling workflow

IN-SITU STRESS DETERMINATION

Fig. 12 shows the stress and pore pressure curves used as input for the hydraulic fracturing model. Vertical (overburden) stress (dashed black line in track 2) was determined by integrating the reconstructed bulk density curve. Pore Pressure (track 1) was estimated based on a gradient plus a pressure offset value that represents the amount of overpressure. Minimum horizontal stress (solid line in track 2) was calculated by using the vertical stress, pore pressure and the static rock elastic properties obtained from the workflow proposed in this work.

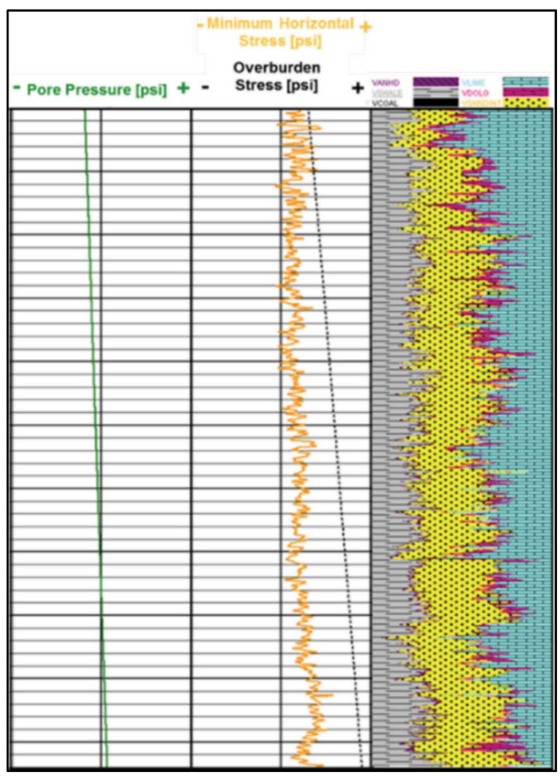

Figure 12. Pore pressure and in-situ stresses

MODEL CALIBRATION

Results from DFIT analysis served as the reference for calibrating pore pressure, minimum horizontal stress and formation permeability. As shown in Fig. 13, typical pre-closure diagnostic techniques (G-function analysis and Log(Δp) vs. Log (Δt) plot) were applied for theassessment of fluid leak-off characteristics and various reservoir parameters, such as fracture gradient, closure pressure, net extension pressure (*i.e.*, process zone stress, PZS), fluid leak-off rate and fracture leak-off mechanism (*i.e.*, pressure dependent leak-off, fracture storage).

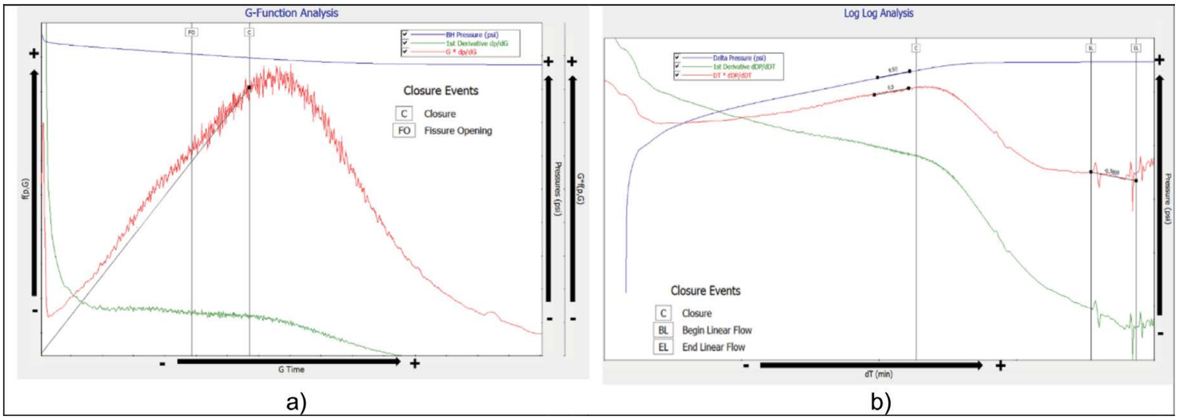

Figure 13. Pre-closure Analysis Diagnostic plots a) G-function plot b) Log-log plot

As an example, fracture closure pressure values from pre-closure analysis were used to calibrate the minimum horizontal stress profile shownin Fig. 12. In addition, G-closure times were used to estimate an overall effective permeability, following Eq. 22 (Barree *et al.*2009), which allowed for a calibration of the permeability model.

$$k = \frac{0.0086\mu\sqrt{0.01\,PZS}}{\varphi c_t\left(^{G_c\,E\,r_p}/_{0.038}\right)^{1.96}} \qquad (22)$$

Where, k is the effective (system) permeability to reservoir fluid (mD); μ is the viscosity of injected fluid, (cP); *PZS* is the process zone stress, the net fracture extension pressure above closure pressure (psi); ϕ is the effective porosity (fraction); ct is the total reservoir compressibility (1/psi); E is the Young's Modulus (MMpsi); r_p is the storage ratio, which corrects for the amount of excess fluid volume that must be leaked-off to reach fracture closure, for the cases of height recession or transverse storage.

For the cases where the DFIT pressure transient reached pseudo-linear (or pseudo-radial) flow conditions, an estimate of the pore pressure was obtained by applying after-closure analysis (ACA) techniques. Fig. 14 shows an example of this type of analysis corresponding to a pseudo-linear flow regime, which was identified by a ½ slope of the pressure derivative in the ACA log – log plot (green line in Fig. 14a). The pore pressure was iteratively determined by extrapolation of the straight pressure line, as shown in Fig. 14b. When the correct pore pressure was selected, the pressure difference curve (pressure minus the estimated reservoir pressure, blue line in Fig. 14a) also followed a ½ slope with a magnitude of 2x the derivative.

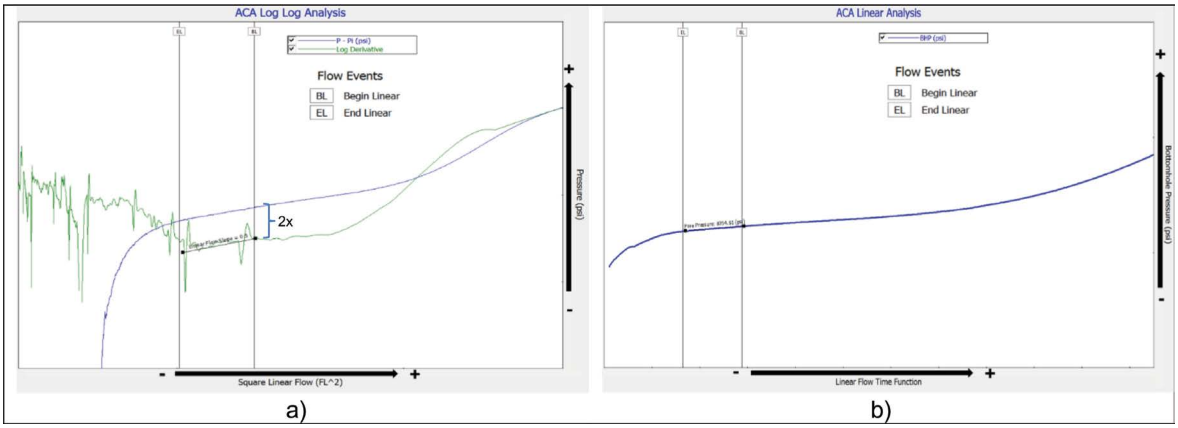

Figure 14. After Closure Analysis (ACA) Diagnostic plots a) ACA Log Log Analysis b) ACA Linear Analysis

Additional calibrations points for PZS and critical fissure opening pressure (CFOP, or pressure above the closure pressure required to open natural fractures) were also obtained from DFIT analysis. Fig. 15 shows the calibrated curves of permeability, PZS, CFOP, pore pressure and minimum *in-situ* stress.

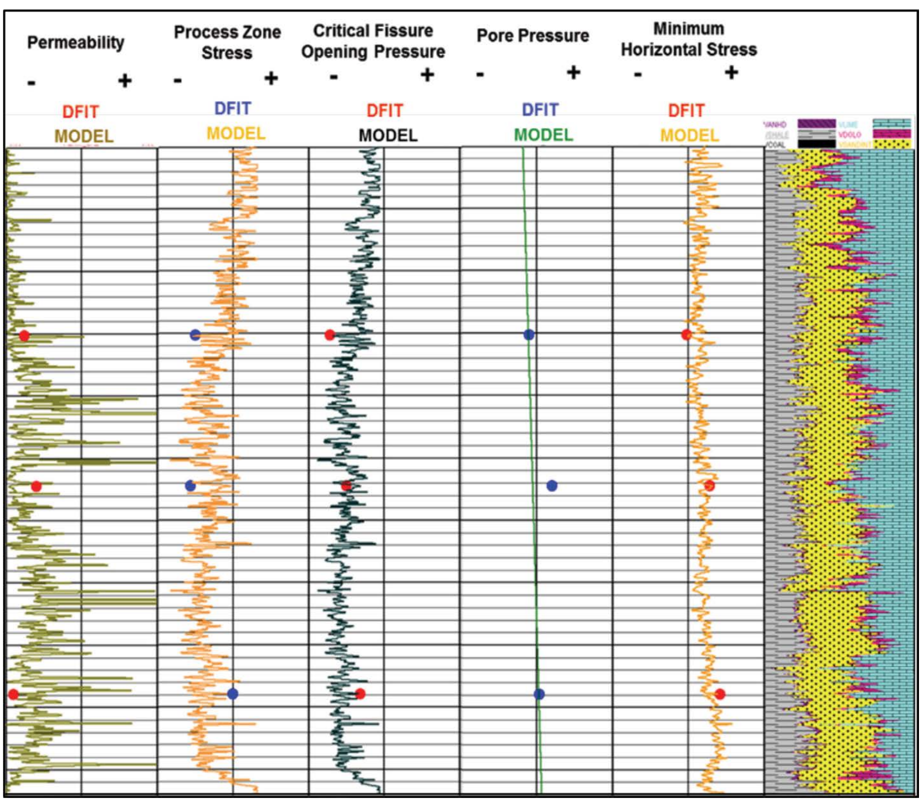

Figure 15. Permeability and stress model calibration using DFIT data.

MODEL VALIDATION

A validation of the stress (and permeability) model was achieved by performing amatch of the surface treating pressure for both the pre-frac and the main frac injections, as shown in Fig. 16. The pressure match obtained, particularly the match of the instantaneous shut-in pressures (ISIP's) and the match of the pressure decline following the DFIT injections, may indicate that the model is being able to capture and reproduce the physical behaviors that are actually occurring in the reservoir.

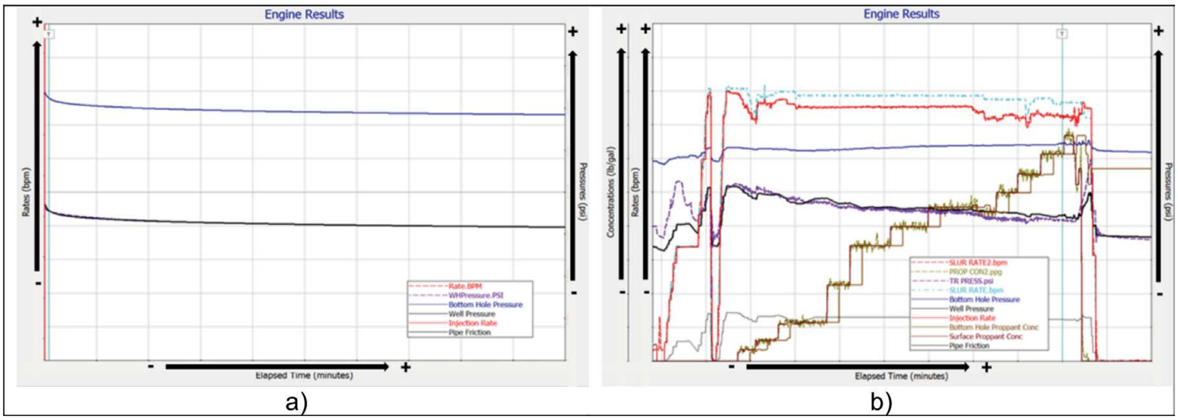

Figure 16. Surface treating pressure match a) pre-frac injection; b) main frac treatment

In addition to pressure calibration (*i.e.* pressure match), calibration to a geometric measurement is needed to reduce model uncertainty. An estimate of the propped fracture height of each hydraulic fracture stagewas obtained by running a cross dipolar-sonic tool before and after the fracturing operation. In this technique, the propped height is correlated to the change in induced shear anisotropy. Since no telemetry tool was included in the logging run, the fast-shear azimuth was not determined. As shown in Fig. 17, for two analyzed vertical wells in Vaca Muerta Formation, there is a good match between the propped fracture height predicted from the hydraulic fracture simulation, based on proppant concentration around the near wellbore area, and the fracture height interpreted fromsonic anisotropy analysis.

A final validation of the hydraulic fracture modelinvolvedperforming production analysis and production matching. First, Rate Transient Analysis (RTA), Fig. 18, was used to determine thereservoir'sdrainage area and aspect ratio, and consequently the estimated ultimate recovery (EUR). From type curve matching, it is observed that the well is entering boundary dominated flow (*i.e.*, the plotted data follows a unit slope). In addition, the analysis allowed to get estimates of permeability, skin or effective fracture half-length. The RTA's derived reservoir permeability agrees with the average NMR permeability of the whole Vaca Muerta section.

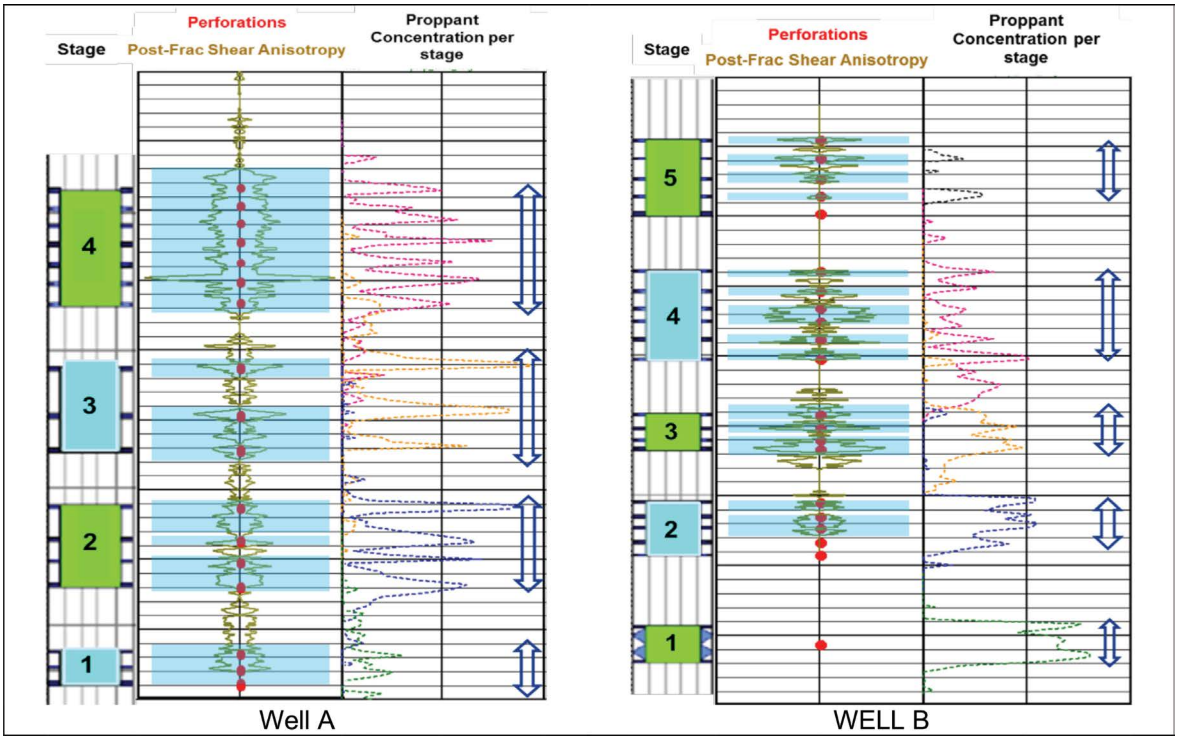

Figure 17. Comparison between simulated propped fracture height and the propped fracture height from sonic anisotropy analysis.

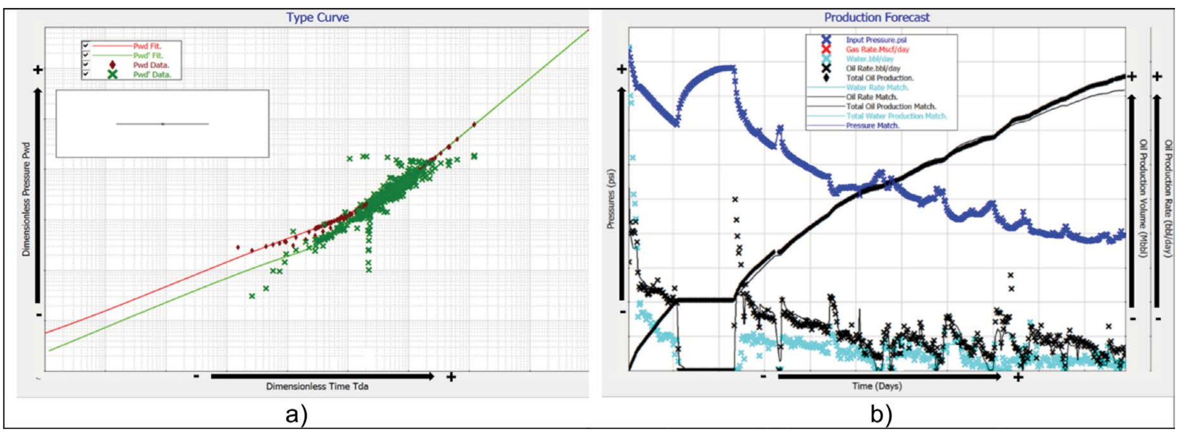

Figure 18. Results from Rate Transient Analsyis (RTA).

Lastly, using the validated permeability and stress models, a match of the production rate and current cumulative production was obtained (Fig. 19). The predicted 5-year total cumulative production is consistent with the estimated EUR from RTA.

CONCLUSIONS

The workflow presented here is an alternative method for estimating the complete elastic stiffness tensor in the case of organic-rich shales formations by integrating results from petrophysical analysis and

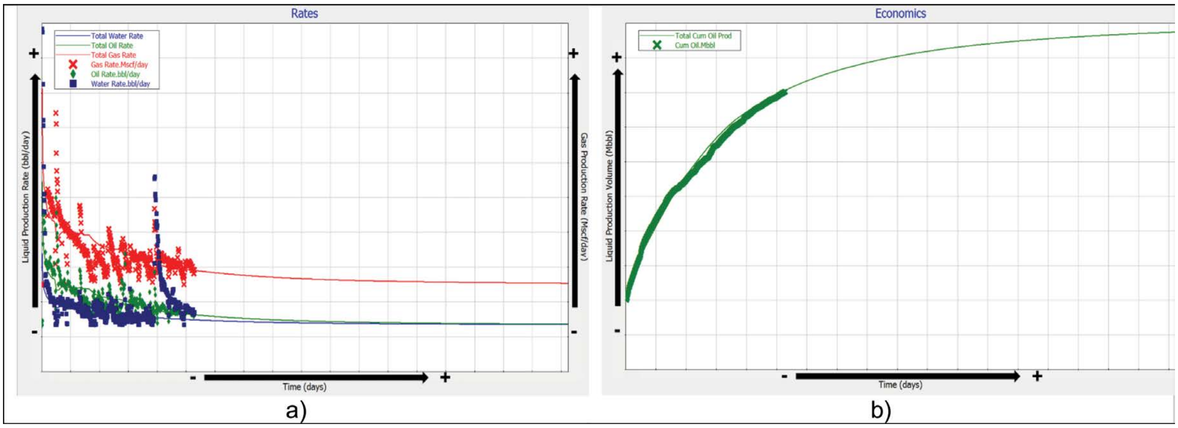

Figure 19. a) Production rate match; b) Cumulative production match.

rock physics principles. The modelled data incorporates compositional (proportions of the constituent components) and textural characteristics (geometric aspects on how the components are arranged relative to each other). Since the modelled data has the same resolution as the results from the petrophysical analysis, it is possible to improve the consistency between elastic moduli and petrophysical properties.

The approach presented here does not rely on original well logs for estimating the elastic moduli, so it can be used in wells with any deviation, provided that a petrophysical analysis is available.

Reconstruction of density and sonic logs provides an additional tool for assessing the quality of the original well logs.

The results of the workflow were applied to the construction of a geomechanical model, which was then used as input for the simulation of hydraulic fracturing in the Vaca Muerta Formation. The application of the proposed workflow resulted in the development of predictive fracture models that were able to reproduce the job treating pressures, and also to match the estimated fracture geometry (*i.e.*, fracture height) and actual post-frac well production. These results provide confidence in the robustness of the method proposed in this work.

Calibration of petrophysical and geomechanical models is required as part of the hydraulic fracturing simulation workflow. Fracture closure pressure (minimum *in-situ* stress), reservoir permeability and pore pressure should be properly estimated from DFIT data analysis (pre-closure and after-closure analyses) and used along with other fracture diagnostic technologies (*e.g.*, production analysis, production logging, radioactive/chemical tracers, microseismic) to constrain and validate the output of the fracture simulator.

ACKNOWLEDGEMENTS

The authors would like to thank Wintershall Energía S.A. and Wintershall Holding GmbH for supporting this work and authorizing the publication of this paper. We also thank and Gas y Petróleo Neuquén S.A. for authorizing the publication of this paper.

REFERENCES

Barree, R.D., Barree, V.L., and Craig, D.P., 2009, "Holistic Fracture Diagnostics: Consistent Interpretation of Prefrac Injection Tests Using Multiple Analysis Methods", SPE Prod & Oper 24(3): 396-406. SPE 107877-PA. DOI 10.2118/107877-PA.

Batzle, M., Wang Z., 1992, "Seismic properties of pore fluids, Geophysics", 57(11), 1396 –1408, doi:10.1190/1.1443207.

Brie, A., Pampuri, F., Marsala, A.F., and Meazza, O., 1995,"Shear sonic interpretation ingas-bearing sands", SPE, 30595, 701–710.

Brown, R., Korringa, J., 1975, "On the dependence of the elastic properties of a porous rock on the compressibility of the pore fluid", Geophys., 40, 608–616.

Canady, W. J., 2011,"A Method for Full-Range Young Modulus Correction", Society of Petroleum Engineers. doi:10.2118/143604-MS

Carcione, J.M., Avseth, P., 2015,"Rock-physics templates for clay-rich source rocks", Geophysics, 80, 481-500, doi: 10.1190/GEO2014-0510.1

Krief, M., Garat, J., Stellingwerff, J., & Ventre, J., 1990, "A Petrophysical Interpretation Using the Velocities of P and S Waves (Full-Waveform Sonic)", Society of Petrophysicists and Well-Log Analysts.

Massaro, A., Espinoza, N., Frydman, M., Barredo, S., Cuervo, S., 2017, "Analyzing a suitable elastic geomechanical model for Vaca Muerta Formation", Journal of South American Earth Sciences, 79, 472-488, doi: 10.1016/j.jsames.2017.09.011

Mavko, G., Mukerji, T., and Dvorkin, J., 2003,"The Rock Physics Handbook", Cambridge, UK: Cambridge University Press.

Prioul, R., Frydman, M., & Caniggia, J., 2016, "Estimating Anisotropic Mechanical Properties and Stress Based on Measurements on Cuttings for Completion Quality: Methodology and Case Study in Vaca Muerta". Society of Petroleum Engineers. doi:10.2118/180969-MS

Quirein, J., Eid, M., Cheng, A., 2014, "Predicting the Stiffness Tensor of a Transversely Isotropic Medium When the Vertical Poisson's Ratio is Less Than the Horizontal Poisson's Ratio", Society of Petrophysicists and Well-Log Analysts.

Sayers, C. M., 2013, "The Effect of Kerogen on the AVO Response of Organic-Rich Shales", Society of Exploration Geophysicists.

Schlumberger, 2015, "Sonic Scanner Processing Report", Internal report prepared for Wintershall Energia S.A.

Tang, X. M., Patterson, D.,2004, "Estimating Formation Permeability and Anisotropyfrom Borehole Stoneley Waves", Society of Petrophysicists and Well-Log Analysts.

Vernik, L., Nur, A., 1992, "Ultrasonic velocity and anisotropy of hydrocarbon source rocks", Geophysics, 57, 727–735, doi: 10.1190/1.1443286.

Vernik, L., Liu, X.,1997, "Velocity anisotropy in shales: A petrophysical study", Geophysics, 62, 521–532, doi: 10.1190/1.1444162.

Vernik, L., Liu, X., Nur, A., 1994, "Effect of Kerogen On Velocity Anisotropy in Source Rocks", Society of Exploration Geophysicists.

Vernik, L., Milovac, J., 2011, "Rock physics of organic shales", The Leading Edge, 30 (3), 318–323.

Vernik, L., 2016, "Seismic Petrophysics in Quantitative Interpretation", Investigations in Geophysics. SN- 978-1-56080-324-9. Society of Exploration Geophysicists.

Vernik, L., Landis, C., 1996, “Elastic anisotropy of source rocks: Implications for hydrocarbon generation and primary migration”, AAPG Bulletin, 80, 531–544.

Walsh, J., Sinha, B., Donald, A., 2006,“Formation Anisotropy Parameters Using Borehole Sonic Data”, Society of Petrophysicists and Well-Log Analysts.

Willis, M., 2013,“Upscaling Anisotropic geomechanical properties using Backus averaging and petrophysical clusters in the Vaca Muerta Formation”, Master of science degree, Colorado School of Mines.

Yenugu, M., Vernik, L., 2015,“Constraining seismic rock-property logs in organic shale reservoirs”, The Leading Edge.